Automatic Contrail Detection and Segmentation

John M. Weiss, *Member, IEEE*, Sundar A. Christopher, and Ronald M. Welch

***Abstract*—Automatic contrail detection is of major importance in the study of the atmospheric effects of aviation. Due to the large volume of satellite imagery, selecting contrail images for study by hand is impractical and highly subject to human error. It is far better to have a system in place that will automatically evaluate an image to determine 1) whether it contains contrails and 2) where the contrails are located. Preliminary studies indicate that it is possible to automatically detect and locate contrails in Advanced Very High Resolution Radiometer (AVHRR) imagery with a high degree of confidence.**

Once contrails have been identified and localized in a satellite image, it is useful to segment the image into contrail versus noncontrail pixels. The ability to partition image pixels makes it possible to determine the optical properties of contrails, including optical thickness and particle size. In this paper, we describe a new technique for segmenting satellite images containing contrails. This method has good potential for creating a contrail climatology in an automated fashion.

The majority of contrails are detected, rejecting clutter in the image, even cirrus streaks. Long, thin contrails are most easily detected. However, some contrails may be missed because they are curved, diffused over a large area, or present in short segments. Contrails average 2–3 km in width for the cases studied.

***Index Terms*— Advanced Very High Resolution Radiometer (AVHRR), jet contrails, remote sensing.**

I. Introduction

THE RADIATIVE energy budget of the earth-atmosphere system is in delicate balance between the incoming solar energy and the outgoing longwave radiation. The incoming solar energy is attenuated by clouds, aerosols, and other particles in the atmosphere, and the outgoing longwave radiation is absorbed and reemitted by gases and these particulates. With increasing trace gas emissions from anthropogenic sources, there is a growing concern about greenhouse warming and possible climate change implications. NASA's Earth Observing System (EOS), to be launched in 1999 [1], is dedicated to understanding these complex interactions between the earth-atmosphere system.

The study of jet contrails is of major importance to a wide range of disciplines, from military planners to climate researchers. Contrails, that form at the wake of jet aircraft, act as tracers that may serve as potential intelligence to military planners. In terms of atmospheric effects, climate researchers are interested in the radiative effects of jet aircraft emissions. Recently, it has been shown that the radiative forcing of surface temperature is about 30 times more sensitive to aircraft emissions of nitrogen dioxide than to surface emissions alone [18]. Jet contrails also are an important subset of thin cirrus clouds in the atmosphere. Thin cirrus clouds are thought to be enhancers of the greenhouse effect due to their semitransparent nature [29]. They are nearly transparent to the solar energy reaching the surface, but they reduce the planetary emission to space due to their cold ambient temperatures. However, a quantitative assessment of the degree to which jet contrails perturb the radiative balance of the earth-atmosphere system still is lacking.

Subsonic aircraft, which fly at an altitude between 8 and 13 km, have continued to increase through the years [7]. The emissions from these aircraft, which include NO_X, CO_X, CO, HC, CO_2, soot, and water vapor [31], lead to contrail and aerosol formation [24]. Pitchford *et al.* [25] argue that if the upper tropospheric and lower stratospheric (UT/LS) buildup of exhaust emissions continues to increase, photochemical reactions and surface changes of these particles could enhance CCN formation. This would lead to enhanced opacity of cirrus clouds formed from such conditions. Having "seeded" the environment, contrails often elongate and widen into cirrus-like features. Joseph *et al.* [20] used Earth Resources Technology Satellite (ERTS) photographs and found contrails with widths up to 100 km. Contrail widths of 5–30 km are seen in Advanced Very High Resolution Radiometer (AVHRR) images, but the average width is 2–3 km.

Considerable uncertainty exists regarding the impact of contrails on surface temperature and precipitation [4]–[6], [9], [13]. Changnon analyzed records of monthly sky cover, temperature, and sunshine for 1901–1977. An area in the central United States that has experienced large increases in jet traffic was found also to have shifted to cloudier, less sunny conditions. Temperatures also decreased during this period, leading to the suggestion that these anomalous changes were due to jet-induced cirrus. Detwiler [9] argued that contrails tend not so much to increase cloudiness but to enhance the formation of natural cloudiness. In one of the earlier works on the interaction of contrails with thermal radiation, Kuhn [22] showed that a 500-m-thick contrail sheet increases the infrared emission below the sheet by 21% and decreases the solar radiation below the sheet by 15%, thereby leading to a net incoming power depletion at the earth's surface by about 7%. Assuming contrail persistence, this results in a 5.3 °C temperature decrease at the earth's surface. Kuhn argued that if jet operations were prevalent in the upper troposphere, where saturation with respect to ice is fairly frequent, the chances for persistence of jet contrails are considerably higher than those in the stratosphere; this is in spite of the fact that the particles

Manuscript received November 7, 1996; revised June 23, 1997. This work was supported by NASA under Grant NAG 5-2712.

J. M. Weiss is with the Department of Mathematics and Computer Science, South Dakota School of Mines and Technology, Rapid City, SD 57701-3995 USA (e-mail: jweiss@silver.sdsmt.edu).

S. A. Christopher and R. M. Welch were with the Institute of Atmospheric Sciences, South Dakota School of Mines and Technology, Rapid City, SD 57701-3995 USA. They are now with the Department of Atmospheric Sciences, University of Alabama at Huntsville, Huntsville, AL 35899 USA.

Publisher Item Identifier S 0196-2892(98)04972-9.

from the engine emissions have a short residence time. The current (and projected) fleet of subsonic aircraft operate in the upper troposphere, thereby increasing the possibilities of persistent contrail formation that could possibly lead to changes in the radiation balance.

Contrails have been regularly observed in satellite imagery [4], [5], [8], [19], [28]. The spectral capabilities of the AVHRR sensor was utilized by Lee [23] to produce images with enhanced contrails. Travis [30] zoomed satellite images and then manually counted pixels to determine the width, length, and areal coverage of contrails. A first attempt at automated detection of contrails was performed by Engelstad *et al.* [12]. The present investigation extends this approach and identifies contrail pixels in an image. Section II provides background on the subject, and Section III describes the methodology. Section IV presents the results, and Section V concludes.

II. Background

The AVHRR channels 4 and 5 are centered in the 10.8- and 12.0-μm atmospheric window regions, respectively. Because these wavelengths are spectrally close, most features radiate similarly in the two channels and are therefore suppressed in the difference image. However, contrails, as well as certain cirrus clouds, are enhanced in this difference image, making subsequent contrail detection much easier.

AVHRR imagery has a spatial resolution of 1.1 km at nadir. In the channel 4–5 difference image, contrails are characterized as thin, nearly straight linear features of higher intensity than the background. Thin features in an image are known as *ridges* when they are of higher intensity than the background [15]. Contrails can be enhanced further in the channel 4–5 difference image by first applying a ridge detection operator [12]. This operator enhances thin linear features in the difference image, eliminating much of the noncontrail data (including many cirrus clouds).

Contrails possess another highly characteristic feature; they tend to create straight lines in satellite images. There are a number of schemes for detecting straight lines in an image, the best known of which is undoubtedly the parametric Hough transform [11], [16]. In order to detect contrails, the Hough transform is applied to the channel 4–5 difference image, after enhancement by the ridge operator. This results in an automated technique for contrail detection in satellite imagery [12].

After contrail detection, it is useful to segment the image into contrail versus noncontrail pixels. Then it becomes possible to retrieve further information concerning contrail optical properties and their contributions to radiative forcing. The Hough transform produces a list of straight line segments in the image that are approximately coincident with the contrails. However, contrails may vary in thickness, may not lie directly beneath the Hough line segments, and may have regions in which they dissipate entirely. Additional processing is required for segmentation, even after the Hough transform has successfully detected the presence of image contrails.

There are several ways in which segmentation may be accomplished. In this study, we present an approach similar to *searching near an approximate location* [2]. Given the approximate location of a contrail from the Hough transform, we examine the image directly beneath and perpendicular to the Hough line segment for contrail pixels.

TABLE I
TABLE OF AVHRR LAC 512 × 512 PIXEL IMAGES USED IN THIS STUDY WITH THEIR LOCATIONS AND DATES

Date	Sat-ID	Orbit #	Center Latitude	Center Longitude	Figure
07/05/88	NOAA-F/9	1 834 747	47.35N	136.76W	7a
07/05/88	NOAA-F/9	1 834 747	45.81N	141.92W	6a
07/05/8	NOAA-F/9	1 834 747	41.18N	142.33W	7b
07/06/88	NOAA-F/9	1 837 070	69.82N	41.33W	6b
07/06/88	NOAA-F/9	1 837 070	71.39N	30.96W	7c
10/01/92	NOAA-H/11	2 587 071	65.07N	22.43W	9a
10/04/93	NOAA-H/11	2 590 808	59.97N	122.42E	8a
10/04/93	NOAA-H/11	2 591 112	61.07N	20.00E	9b
10/04/93	NOAA-H/11	2 591 112	54.61N	19.45E	9c
10/07/93	NOAA-H/11	2 595 151	53.96N	70.02E	8b
10/07/93	NOAA-H/11	2 595 151	59.09N	74.43E	8c
10/01/92	NOAA-H/11	2 587 071	38.91N	09.44W	6c

III. Methodology

A. Data and Preprocessing

In this study, 12 AVHRR Local Area Coverage (LAC) images are used to develop the detection algorithm. Table I shows the regions and times over which the images were acquired. The AVHRR sensor has a nominal spatial resolution of about 1 km at nadir and five spectral channels [21] (0.58–0.68 μm, 0.72–1.1 μm, 3.55–3.93 μm, 10.3–11.3 μm, and 11.5–12.5 μm). The infrared channels (channels 4 and 5) are calibrated onboard. However, the calibration scheme is not completely linear. Nonlinear calibration of the infrared channels is performed following Brown *et al.* [3]. Since the visible and near-infrared channels (channels 1 and 2) do not have any online calibration, postlaunch calibration coefficients [27] are used to correct for degradation effects. Channels 1 and 2 are converted to albedos, and channels 3–5 are converted to temperatures [21].

B. Difference Images

Figs. 1–3(a)–(e) show the five channels for three 512 × 512 pixel regions from different AVHRR images containing contrails. The 10-bit values have been calibrated and then mapped into 8 bits for display purposes. Also, linear contrast stretching [17] is applied to enhance the contrast. Histogram equalization [14] is an alternative approach for visualizing contrails in AVHRR imagery.

Fig. 1 shows high-altitude contrails as straight line segments over an underlying stratus cloud layer. The darker straight line segments seen in Fig. 1(a) and (b) may be contrail shadows on

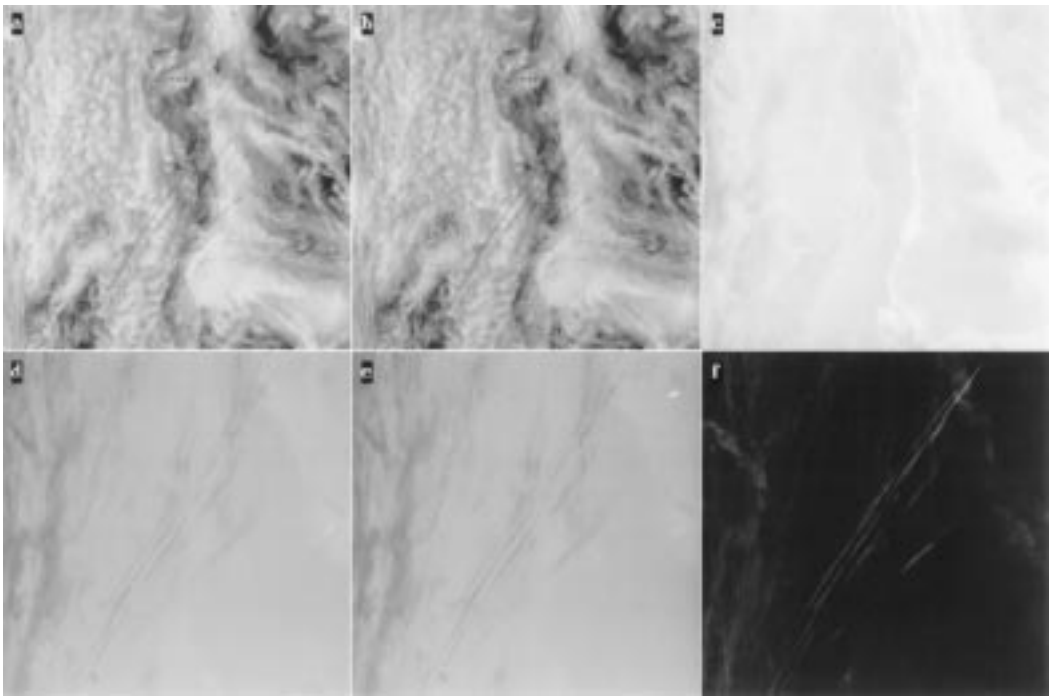

Fig. 1. AVHRR contrail image: (a) channel 2, (b) channel 2, (c) channel 3, (d) channel 4, (e) channel 5, and (f) channel 4–5 difference.

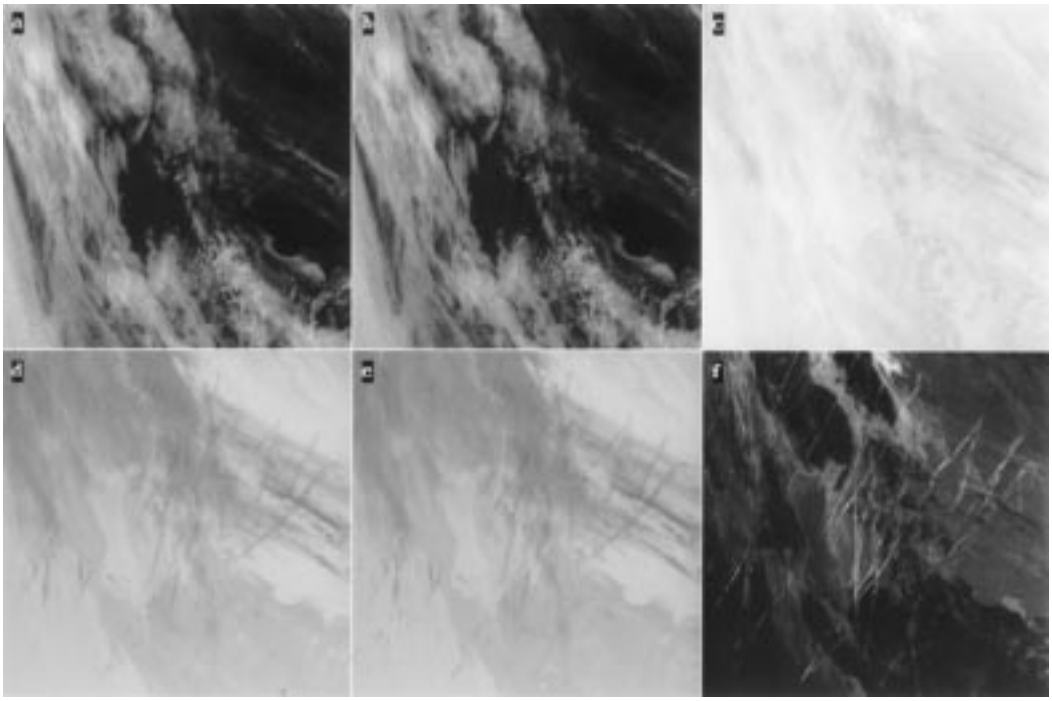

Fig. 2. AVHRR contrail image: (a) channel 1, (b) channel 2, (c) channel 3, (d) channel 4, (e) channel 5, and (f) channel 4–5 difference.

the underlying cloud deck. Such features are not observable in Figs. 2(a) and (b) or 3(a) and (b) over a dark background in the visible and near-infrared channel 1 and 2 images, respectively. Contrails are not reliably detectable using the mid-infrared channel 3 images, as demonstrated in Figs. 1(c), 2(c), and 3(c). However, they are discernible as dark streaks in the infrared channel 4 and 5 images, as seen in Figs. 1(d) and (e)–3(d) and (e).

The first step in contrail detection and segmentation is generation of the channel 4–5 difference image. It has been shown, both in this laboratory [12] and elsewhere [23], that subtracting AVHRR channel 5 from channel 4 produces an image in which contrail signatures are greatly enhanced.

The calibrated pixel values in channels 4 and 5 represent temperatures, typically between 180 and 327 K. However, the resulting difference image has extremely low contrast, since the difference values are often less than 8 K. Some form of contrast enhancement is essential to visualize the contrails in the difference image. Figs. 1–3(f) show the channel 4–5 difference images corresponding to the

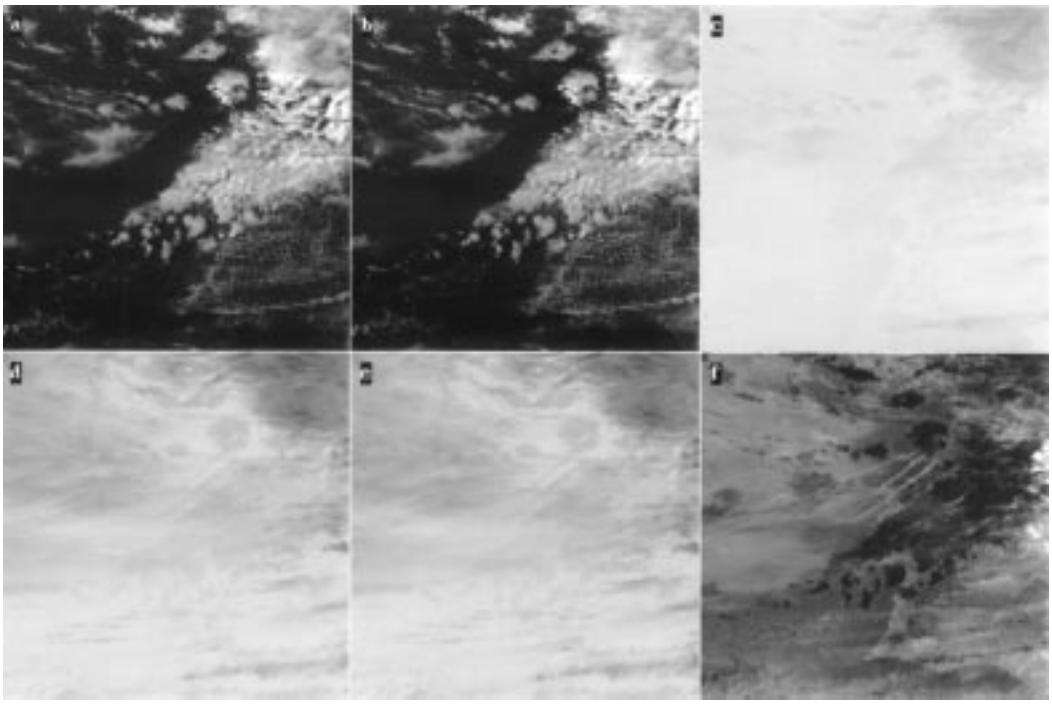

Fig. 3. AVHRR contrail image: (a) channel 1, (b) channel 2, (c) channel 3, (d) channel 4, (e) channel 5, and (f) channel 4–5 difference.

512×512 regions of Figs. 1–3(a)–(e), after applying linear contrast stretching. Note the dramatic enhancement of contrails, and suppression of many other image features. Many contrails that were hidden by other image features are visible in the difference image.

C. Ridge Classification

Classification of pixels into ridges provides candidates for contrail identification, making contrail detection via the Hough transform more robust. A ridge is a connected linear structure that is very long relative to its width, with a skeleton along which the pixel intensities change slowly [15]. Ridge points are brighter than the surrounding background in at least two directions. The ridge width need not be constant, but it should change slowly (if at all).

Contrails form ridges in the channel 4–5 difference images (Figs. 1–3). A ridge operator is used to eliminate many non-contrail pixels from these contrail-enhanced images. Our ridge operator is based on two observations. First, the definition of a ridge requires that every point along the ridge is a local maximum in at least one direction (perpendicular to the ridge). Second, inside a small neighborhood, a digital ridge may be oriented in one of four directions: horizontally, vertically, or along the two diagonals.

The ridge-finding algorithm used for contrail detection is described in detail in [12]. This algorithm examines a 6×6 neighborhood for horizontal, vertical, and diagonal ridges. The 6×6 neighborhood was specifically selected for detection of contrails in AVHRR imagery. Jet contrails are seldom more than 3 km wide [10], so ridges tend to be three pixels wide or less, and they are readily detectable inside a 6×6 neighborhood.

Inside this 6×6 neighborhood, nine values are computed by summing groups of four adjacent pixels. The central pixel in the neighborhood is classified as a ridge if three of the nine values form an elevated line in one of four possible ridge orientations. The ridge orientation may be in a horizontal, vertical, or diagonal direction, as follows:

$$\begin{matrix} 0&0&0 \\ 1&1&1 \\ 0&0&0 \end{matrix} \quad \begin{matrix} 1&0&0 \\ 0&1&0 \\ 0&0&1 \end{matrix} \quad \begin{matrix} 0&1&0 \\ 0&1&0 \\ 0&1&0 \end{matrix} \quad \begin{matrix} 0&0&1 \\ 0&1&0 \\ 1&0&0. \end{matrix}$$

The three values along the line (the ones) must be greater than the values alongside the line (the adjacent zeros), since the ridge definition requires a local maximum perpendicular to the ridge direction.

The ridge location and direction are stored for later use in the Hough transform. The ridge direction is given by the maximum response of the ridge operator; i.e., whichever of four ridge orientations is maximally elevated over its neighboring values. A pixel is classified as belonging to a ridge only when the ridge operator response exceeds a threshold, as discussed in Engelstad *et al.* [12]. Fig. 4(a)–(c) shows the ridges found in the contrail-enhanced images of Figs. 1–3, respectively.

At this point, we have an image in which the features of interest (contrails) have been greatly enhanced with respect to the original AVHRR imagery. These are the long line segments seen in Fig. 4(a)–(c). However, there are significant numbers of other bright points and short line segments that constitute noise. There remains the problem of detecting and locating the contrails. To do so, we make use of the fact that contrails tend to form straight lines in satellite images.

D. Hough Transform

Consider the general problem of detecting and locating a straight line in an image. After performing ridge detection, we have a collection of ridge pixels, some of which lie on the line and some of which do not. A straightforward approach

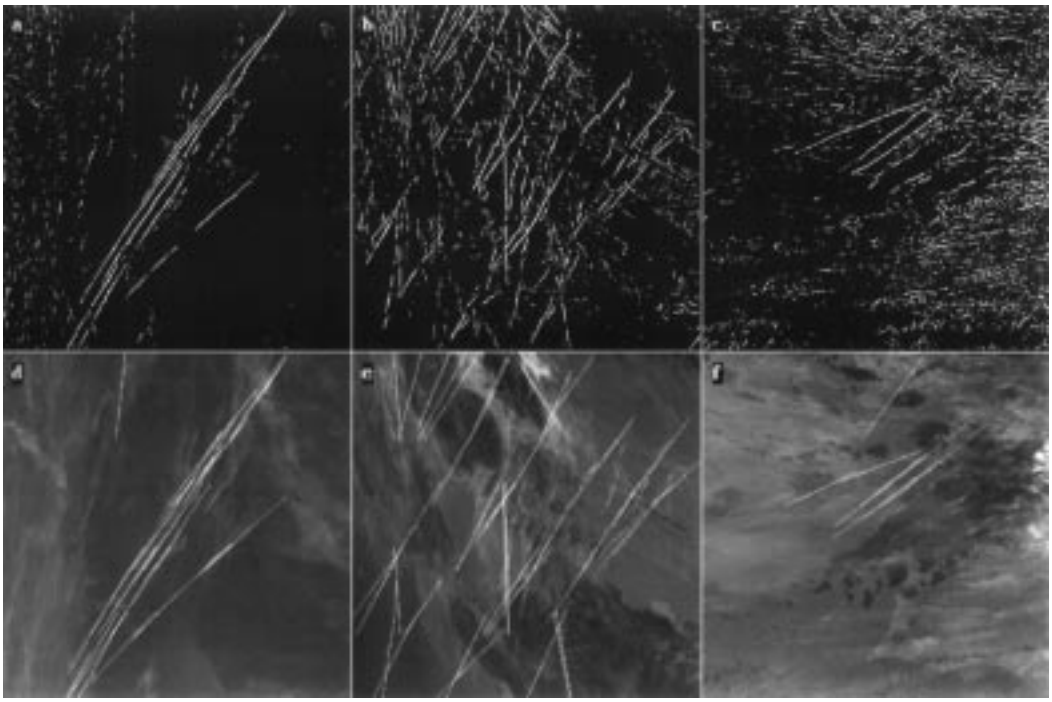

Fig. 4. (a)–(c) Ridge detection applied to AVHRR channel 4–5 difference images and (d)–(f) Hough line detection superimposed upon AVHRR channel 4–5 difference images.

would involve counting how many ridge pixels lie along each possible line. The line with the greatest number of ridge pixels corresponds to the actual line in the image.

Unfortunately, this approach is computationally prohibitive. Given N ridge pixels, there are $N(N-1)/2$ possible lines. Comparing every ridge pixel to every line leads to an $O(N^3)$ algorithm, in which N could be a substantial fraction of all the image pixels.

A more efficient approach was originally proposed by Hough [16]. In its most basic form, the Hough transform maps a point (x, y) into a line in Hough parameter space (m, b). The parameters m and b correspond to the slope and intercept of a line, from the parametric equation $y = mx + b$. Collinear points will generate lines in Hough space that intersect at a single point. The parameters (m, b) at this point give the equation of the line.

To implement the Hough transform, a two-dimensional (2-D) accumulator array is set up to represent the Hough parameter space. One dimension represents possible values of the parameter m, and the other dimension represents possible values of the parameter b. The algorithm is as follows:

```
initialize the accumulator array A to zero

run a ridge detector on the image

for each ridge pixel f(x, y) in the image do
      for each value of m do
            compute b = -mx + y
            increment A[m, b]
      endfor
endfor

find maxima in A, corresponding to lines in the image.
```

The above formulation suffers from the problem that the slope m is undefined for vertical lines. Duda and Hart [11] proposed an alternate formulation based on a different parametric equation for a line $\rho = x \cos\theta + y \sin\theta$. In this formula, ρ is the perpendicular distance from the origin to the line and θ is the angle the perpendicular makes with the x-axis. As θ varies from 0 to 360°, the value of ρ is computed and the corresponding location in the accumulator array $A[\rho, \theta]$ is incremented.

Local maxima in the accumulator array indicate straight lines in the image. A local maximum whose value is higher than a given threshold indicates the presence of a contrail. From the values of ρ and θ, it is simple to superimpose the detected line on the image.

Several modifications to the standard parametric Hough technique are used in the present contrail detection scheme. In the classic Hough transform, an edge detector is used to produce candidate line points rather than a ridge detector. Edge pixels are typically found using a digital approximation to the gradient operator (the first derivative), such as the Sobel or Prewitt operators [14]. Edge detectors do not perform as well in this application because they respond to all edges, including cloud boundaries, land-water interfaces, etc. Ridge detectors respond only to thin linear features, such as contrails and thin cirrus streaks, and hence produce fewer false contrail identifications.

There is another advantage to using the ridge operator described in the previous section. Since the ridge operator gives the approximate direction of the line (horizontal, vertical, or diagonal), a computational speedup is possible. Instead of varying θ over 360°, we vary it by only 45° ($\pm$22.5° from the ridge direction). This significantly reduces the amount of processing required to increment the accumulator array.

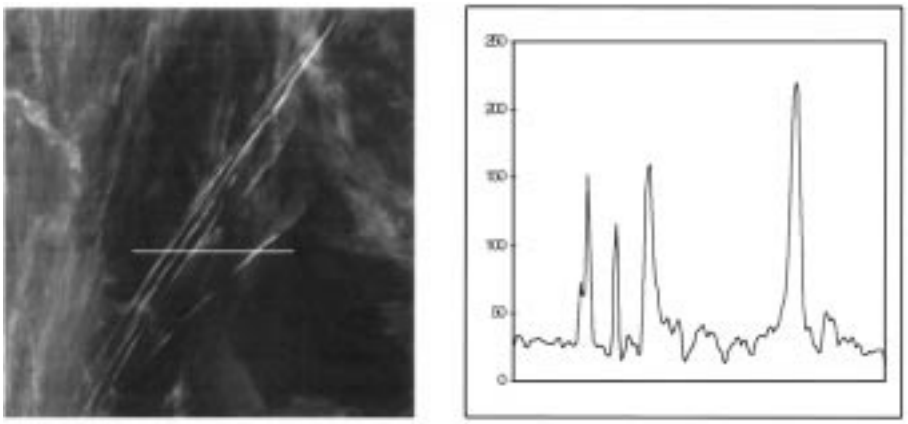

(a) (b)

Fig. 5. (a) AVHRR contrail image (channel-45 difference). Horizontal line yields the intensity profile. (b) Intensity profile showing ridge-like structures that correspond to contrails in the image.

Contrails seldom extend over the entire breadth of an AVHRR image. Better results are achieved by partitioning an AVHRR image into overlapping 128 × 128 subimages and performing the Hough transform individually on each subimage. Line segments that cross subimage boundaries are easily identified and linked together as a postprocessing step.

A major problem in contrail detection is false identification of thin cirrus streaks as jet contrails. Rather than using an absolute threshold for selecting maxima in the accumulator arrays, we apply a dynamic threshold based on the amount of ridge "clutter" in the image [12]. In each of the four possible ridge directions, an adaptive threshold is computed based on the number of ridge pixels oriented in that direction. The threshold is larger when thin cirrus streaks are present, helping prevent false contrail identification. In the absence of cirrus streaks, or in a different direction, the threshold is lower, allowing more sensitivity in contrail detection.

The results of contrail detection by the Hough transform are shown in Fig. 4(d)–(f). Most of the contrails that are observed in the channel 4–5 difference images shown in Figs. 1(f)–3(f) are correctly identified by this technique. However, a few small contrails are not marked as straight lines by the Hough method, and there is at least one cirrus streak that is incorrectly marked as a contrail [Fig. 4(d)]. This is due in part to certain thresholds in the Hough transform, such as the threshold for selecting maxima in the accumulator array. Decreasing this threshold marks more straight line segments, increasing the number of contrails that are marked, but also increasing the number of mismarked cirrus streaks. Increasing this threshold reduces the number of mismarked cirrus streaks, but it increases the number of weak contrails that are not marked as straight lines. This represents the major limitation of the present scheme.

E. Contrail Segmentation

The Hough transform produces a list of straight line segments in the image that are approximately coincident with the contrails. However, the contrails are not necessarily exactly one pixel thick. In some places, they may have spread to be several pixels wide; in others, part of the contrail may no longer be visible. Furthermore, the contrail may not be exactly collinear with the Hough line segment. Additional processing is required for segmentation, even after the Hough transform has successfully detected image contrails.

There are several ways in which segmentation may be accomplished. Perhaps the most straightforward approach is searching near an approximate location [2]. Given the approximate location from the Hough transform, we examine the image directly beneath and perpendicular to the Hough line segments for contrail pixels.

Contrail pixels are characterized by higher intensities than the surrounding pixels in the channel 4–5 difference image. However, it is difficult to identify contrail pixels using an absolute intensity threshold. In some cases, contrails lie over dark ocean; in others, they lie over bright clouds or snow. The resulting intensity values can vary dramatically, even in the channel 4–5 difference image.

Instead, we make use of the characteristic shape of the ridge cross section for searching. A ridge is a long, thin structure, higher in intensity than the background. Along the ridge, pixel intensities may increase, decrease, or stay the same, just as elevations may vary along a ridge line. However, the cross section of a ridge has a characteristic profile that resembles a Gaussian curve, as shown in Fig. 5. Fig. 5(a) shows a horizontal segment arbitrarily selected that crosses four contrails. Fig. 5(b) shows the channel 4–5 difference intensity profile along this segment. The cross-sectional profile features a local maximum (or peak) at the position of each ridge. Pixel intensities drop on either side of the ridge and eventually reach the level of the surrounding background.

By searching in a direction perpendicular to the detected Hough line segments, the characteristic ridge cross-sectional profile may be used to identify contrail pixels. First, the location of the ridge itself must be found. This corresponds to the peak in the cross-sectional profile. We search perpendicularly to locate the peak, which may not lie directly underneath the Hough line segment, but it will certainly be located nearby.

In the ridge cross-sectional profile, pixel intensities decrease rapidly on either side of the peak, as seen in Fig. 5(b). After locating the peak, we search for the beginning of the intensity drop off by examining the difference between

adjacent pixel intensities along the perpendicular. When the difference between two adjacent pixels exceeds a threshold, the beginning of the drop off has been found.

Pixel intensities continue to decrease rapidly in the ridge cross-sectional profile on either side of the peak, but eventually the rate of decrease slows as the edge of the ridge is reached. By continuing to monitor the difference in adjacent pixels along the perpendicular, we detect the end of the drop off. When the difference between two adjacent pixels no longer exceeds a threshold, the end of the drop off has been found.

At this point, we have identified the end of the intensity drop off on either side of the peak in the ridge cross-sectional profile, perpendicular to the detected Hough line segment. All pixels between these two points are marked as contrail pixels. This is done for every pixel on the Hough line segment. Because contrails tend to be fairly narrow, the search process is quite efficient.

There are several cases in which the algorithm will not mark contrail pixels along the Hough line segment. If a local maximum corresponding to the ridge peak cannot be found, the point is rejected as a contrail pixel. This may occur when the contrail has partially dissipated or is obscured by a bright cloud. If the beginning or end of the drop off cannot be found in either direction, once again the point will be rejected as a contrail pixel.

The search algorithm for identifying contrail pixels is the following:

for each Hough line segment
  for each pixel (x, y) along the line segment
    search perpendicularly to the line segment from (x, y) in both directions until a peak is located at (x_p, y_p)
    search perpendicularly to the line segment from (x_p, y_p) to the "left" until the beginning of the "left" drop-off (x_L, y_L) is located
    continue to search perpendicularly to the line segment from (x_L, y_L) to the "left" until the end of the "left" drop-off (x_L, y_L) is located
    search perpendicularly to the line segment from (x_p, y_p) to the "right" until the beginning of the "right" drop-off (x_r, y_r) is located
    continue to search perpendicularly to the line segment from (x_r, y_r) to the "right" until the end of the "right" drop-off (x_r, y_r) is located
    if (x_p, y_p), (x_L, y_L) and (x_r, y_r) are successfully located, mark pixels from (x_L, y_L) to (x_r, y_r) as contrail pixels.

It is also possible to classify ridges into different widths using this segmentation approach. Contrails tend to spread out and widen with time under certain atmospheric conditions. The width of a contrail may yield important information about its duration or the conditions under which it formed and persisted. Segmentation by searching perpendicularly to the detected Hough line segments makes it simple to classify contrails according to width. For each pixel along the line segment, we compute the ridge cross-sectional width to mark contrail pixels. This allows the average contrail width to be readily computed.

F. Other Processing Steps

As mentioned earlier, the channel 4–5 difference image consists of relatively small temperature differences. For processing efficiency and image display purposes, we linearly rescale the data to 8-bit unsigned integer values prior to ridge detection. Temperature differences in the range -1.00 to $+6.65$ °C are rescaled to the integer range 0 to 255. The few values outside this temperature range are simply clipped at 0 to 255. This yields excellent image display results for a wide variety of AVHRR images.

Linear contrast stretching not only improves image display, but it also helps reduce the selection sensitivity of ridge drop-off thresholds. When the ridge "height" relative to the background may be as little as 0.2 °C, results are extremely sensitive to threshold selection. Increasing the ridge "height" relative to the background by roughly 30-fold makes it easier to select general thresholds that work effectively across a wide range of images.

Smoothing [14], [26] is another processing step that improves the results of contrail segmentation. The characteristic ridge cross-sectional profile may be degraded by random noise. Smoothing reduces the noise, yielding superior segmentation results. A centerweighted 3×3 smoothing filter is applied to the channel 4–5 difference image after contrast stretching and prior to segmentation, as follows:

$$\frac{1}{16}\begin{bmatrix} 1 & 2 & 1 \\ 2 & 4 & 2 \\ 1 & 2 & 1 \end{bmatrix}.$$

Centerweighted filters such as these tend to preserve delicate image features better than simple averaging filters. Preprocessing the channel 4–5 difference image with this centerweighted 3×3 smoothing operator tends to spread contrails slightly, but it improves the overall accuracy of segmentation.

IV. Results

Fig. 6(a)–(c) shows three channel 4–5 difference images containing contrails, and Fig. 6(d)–(f) shows the detected segmented contrails overlaid onto these images. As can be seen, the detection and segmentation algorithm is robust in discriminating the majority of contrails in a scene. Fig. 6(a) and (d) shows that the four strong contrails in the center of the image are successfully detected without human intervention. Clutter from an underlying cloud deck, shown in Fig. 1, is rejected. The only false signal appears to be a small streak at the top of the image, labeled "A."

Fig. 6(b) and (e) shows a scene with a large number of contrails. Once again, the majority of contrails are detected, clearly rejecting clutter in the image, even cirrus streaks. Some contrails are missed because they are curved, diffused over a larger area, or present only in short segments. Long, thin

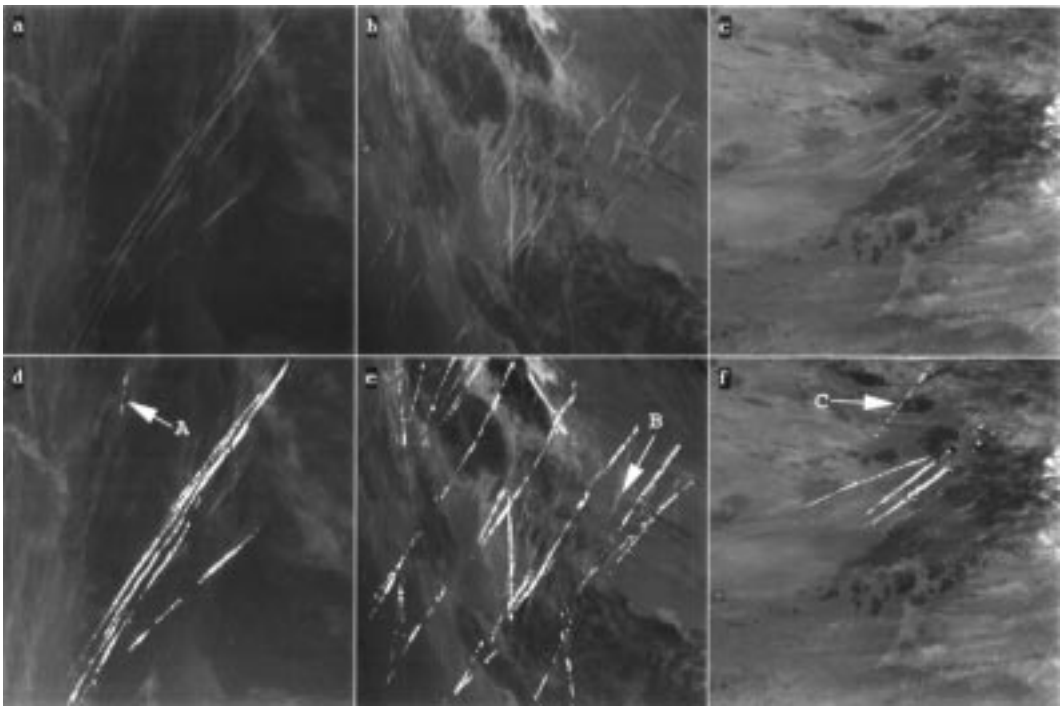

Fig. 6. (a)–(c) Three channel 4–5 difference images. (d)–(f) Images with contrails overlaid.

contrails are most easily detected. The Hough line identification approach is applicable only to straight lines. While it is capable of detecting lines consisting of line segments, the Hough approach may fail if the segments are too sparse. The failure of the algorithm to detect the diffuse contrails, such as the one labeled "B" in Fig. 6(e), may be traced to the 6×6 pixel ridge detection approach. The present results suggest that a larger neighborhood ridge detection scheme be required for diffuse contrails. The reason that a larger neighborhood mask has not been used in this investigation is that it then tends to falsely identify cirrus streaks as contrails. A new approach specifically designed to detect diffuse contrails is under development.

Fig. 6(c) and (f) show three major contrails correctly identified in the center of the scene. Only the line segment labeled "C" appears to be a false detection.

Figs. 7–9 show additional channel 4–5 difference images with detected contrails overlaid. Fig. 7(d) shows that contrails may be successfully detected even when they are closely spaced. In Fig. 7(d), the contrail labeled "A" is not detected due to the fact that it is both faint and curved. Two falsely detected cirrus streaks are labeled as "B" and "C." Thin cirrus streaks that have a ridge structure may be falsely detected as contrails. Fig. 7(e) shows that relatively broad contrails are detected by the algorithm. However, two diffuse contrails labeled "D" and "E" in Fig. 7(e) are not detected, while complicated cloud structure appears to be producing false detections in Fig. 7(f), labeled "F." Nevertheless, a large number of streaks are correctly rejected by the algorithm.

In Fig. 8, contrails are correctly identified except the lines labeled "A" in Fig. 8(d), "B" in Fig. 8(e), and "C" in Fig. 8(f). Some very faint straight lines may be seen in Fig. 8(e) that may be contrails. However, a number of faint linear features are correctly discriminated against in Fig. 8(f). In order to correctly identify the major contrails in an image, Fig. 8 demonstrates that a few thin contrails are missed and a few other linear features may be falsely identified. Nevertheless, the contrails are successfully discriminated, even against a noisy background.

Fig. 9 shows the final three scenes that contain a very cluttered background. Once again, the algorithm is robust in identifying most of the major contrails. Several potential contrails are not identified in Fig. 9(d) and (e), labeled A–E, primarily due to their faint or diffuse nature. Contrail detection is more problematic over cluttered backgrounds because the ridge identification using the 6×6 pixel mask may fail in such cases.

In agreement with Engelstad *et al.* [12], we conclude that while the algorithm is robust in the detection of most contrails, it is less effective when features are weak, diffuse, or curved. Especially difficult are highly cluttered scenes with many cirrus streaks. Increased contrail detection may be achieved but only at the cost of increasing false alarms, while decreasing the number of false alarms necessarily eliminates some faint contrails.

V. Contrail Widths

The method developed by Engelstad *et al.* [12] is successful in detecting the presence of contrails in an image. However, that approach is not capable of discriminating all contrail pixels in the image. The present approach eliminates noncontrail pixels from straight line contrail identifications and segments the contrails for additional processing. This is an essential step if automatic analysis of contrail properties in contrail climatologies is to be achieved.

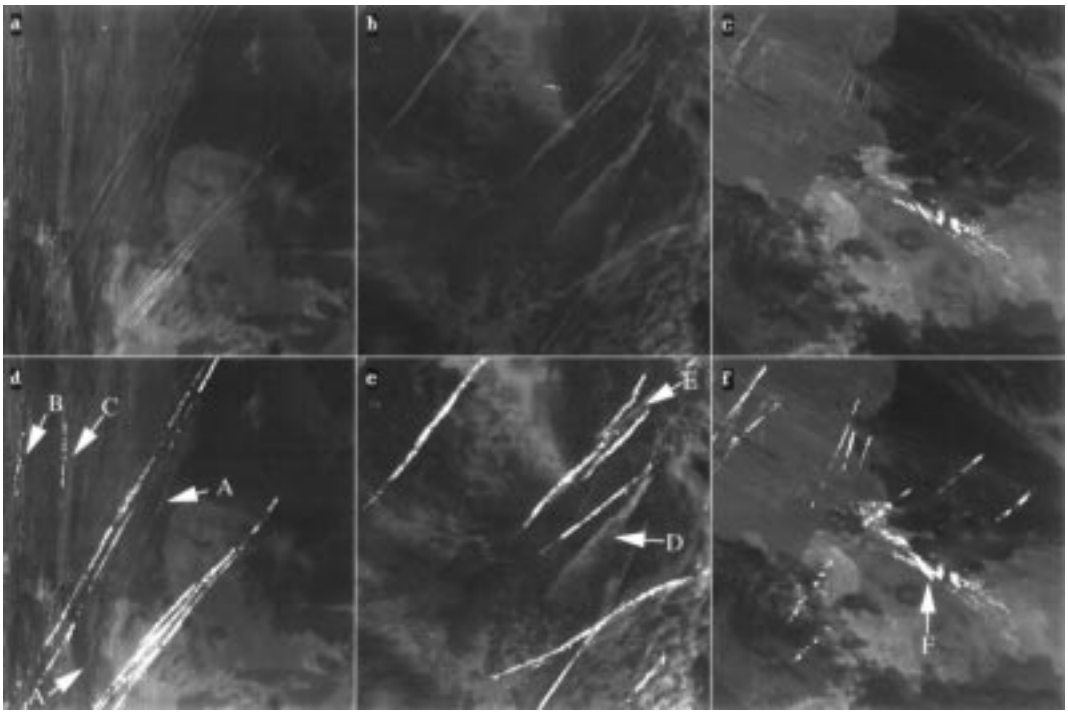

Fig. 7. (a)–(c) Three channel 4–5 difference images. (d)–(f) Images with contrails overlaid.

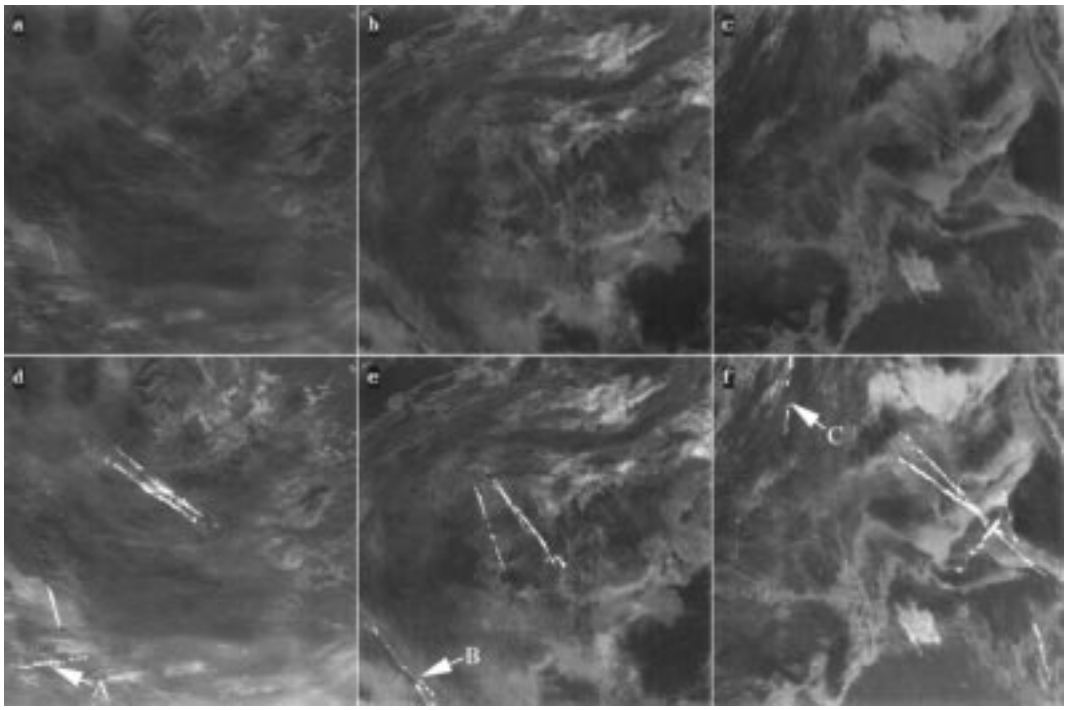

Fig. 8. (a)–(c) Three channel 4–5 difference images. (d)–(f) Images with contrails overlaid.

One important parameter is contrail widths. This information is needed to test the hypothesis that jet contrails spread to create additional upperlevel cloudiness. Such an increase in cloudiness is hypothesized to have important climatological consequences. As a caveat, it should be noted that, in the results presented below, large, diffuse contrails are not included because the present algorithm is designed to discriminate against them. As mentioned previously, a new approach for the detection of diffuse contrails is under development. Therefore, the present results, while valid for the vast majority of contrails observed in the present investigation, are not complete.

Fig. 10 shows contrail widths in terms of pixels for the 12 scenes examined in this investigation. Contrail widths typically show peaks of two pixels in this study. AVHRR imagery is 1.1-km spatial resolution at nadir. However, spatial resolution varies significantly with viewing angle, and contrail widths will vary with orientation within an image; for

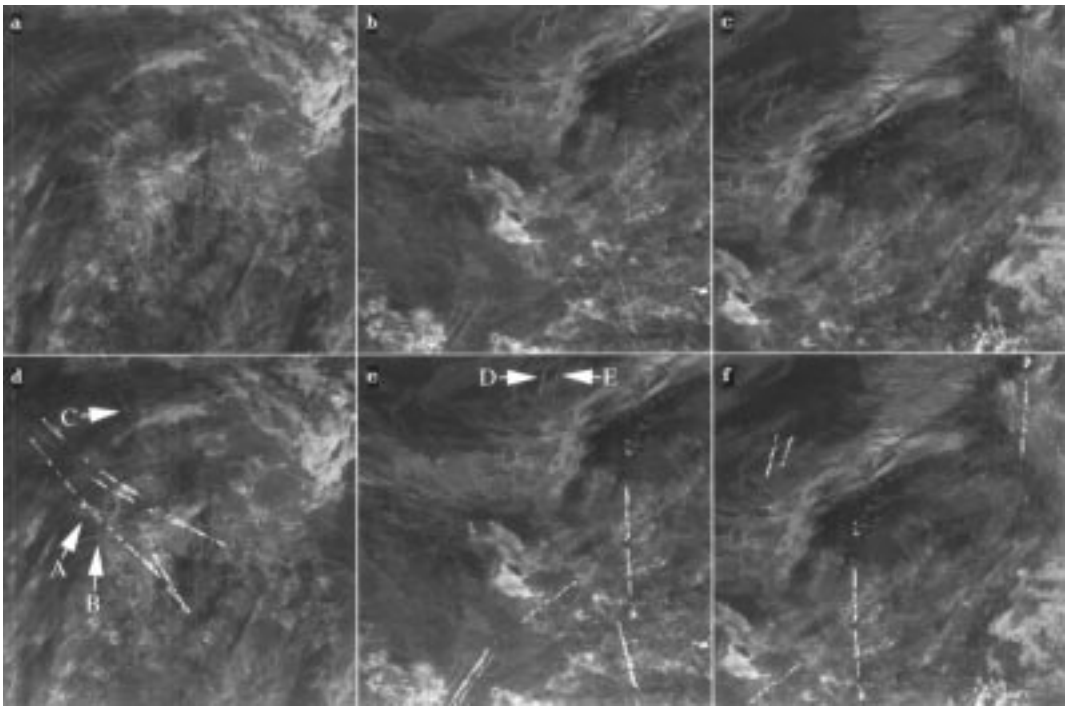

Fig. 9. (a)–(c) Three channel 4–5 difference images. (d)–(f) Images with contrails overlaid.

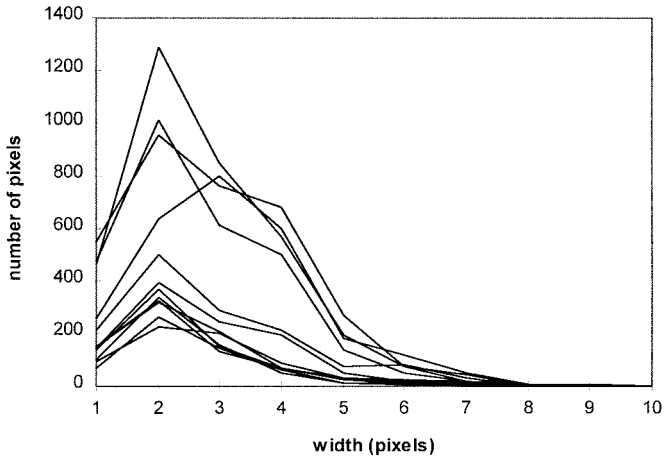

Fig. 10. Histogram of contrail widths in 12 AVHRR scenes.

example, at an orientation of 45°, pixel widths would need to be increased by a factor of 1.4. Taking these factors into consideration, contrail widths in this investigation peak at about 2–3 km, in agreement with Detwiler and Pratt [10] and Travis [30]. In terms of area covered in a 512 × 512 pixel scene, contrails covered from a low of 0.4% to a high of 2.7% of the scenes.

This investigation will be extended to a contrail climatology in the near future. Contrail widths will be computed taking into account viewing geometry and contrail orientation. However, a more robust method for the detection of large, diffuse contrails first must be developed.

In terms of CPU requirements on a 486-66 PC, ridge detection required approximately 6 s for a 512 × 512 region. The Hough algorithm required between 4.8 and 10.3 s, depending upon the number of contrails present. Contrail segmentation took under 0.5 s.

VI. Conclusions

The results presented in this paper show that it is possible to automatically detect and segment contrails in AVHRR images by using the multistep protocol outlined above. For contrail detection, the difference between channels 4 and 5 is used to generate a contrail-enhanced image. Ridge detection eliminates many of the remaining noncontrail pixels. Finally, the parametric Hough transform is applied to overlapping subregions of the contrail-enhanced image to detect contrails.

Once contrails have been detected, segmentation is performed by searching perpendicularly to the maximum at the location of the ridge line, with an intensity drop off to either side. By searching first for the peak and then the boundaries of the drop off, contrail pixels may be identified. The results of this technique thus far have been promising.

The majority of the contrails are detected, clearly rejecting clutter in the image, even cirrus streaks. However, some contrails may be missed because they are curved, diffused over a large area, or present in short segments. Long, thin contrails are most easily detected and segmented with the present algorithm. Increased contrail detection may be achieved, but only at the cost of increasing false alarms. This strategy necessarily eliminates some faint contrails.

A new approach designed to detect diffuse contrails is under development. In addition, a contrail climatology will be compiled. Now that segmentation is achievable, contrail physical properties, such as optical thickness, effective particle size, and emissivity may be retrieved.

Neglecting the large diffuse contrails, the peak in contrail widths, for the 12, 512 × 512 pixel regions investigated, was

2–3 km. The algorithm is relatively efficient, requiring an average of 12 s on a 486-66 PC.

ACKNOWLEDGMENT

Special thanks are extended to D. Kliche and X. Li for their programming help. Appreciation is extended to C. Crandall for typing this manuscript.

REFERENCES

[1] G. Asrar and D. J. Dokken, *EOS Reference Handbook*, NASA NP0202, 1993, p. 145.
[2] D. H. Ballard and C. M. Brown, *Computer Vision.* Englewood Cliffs, NJ: Prentice-Hall, 1982, p. 523.
[3] J. W. Brown, O. B. Brown, and R. H. Evans, "Calibration of Advanced Very High Resolution Radiometer infrared channels: A new approach to nonlinear correction," *J. Geophys. Res.*, vol. 98, pp. 18 257–18 268, 1993.
[4] A. M. Carleton and P. J. Lamb, "Jet contrails and cirrus clouds: A feasibility study employing high resolution satellite imagery," *Bull. Amer. Meteorol. Soc.*, vol. 67, pp. 301–309, 1986.
[5] _____, "Response to comments on 'Jet contrails and cirrus cloud: A feasibility study employing high resolution satellite imagery'," *Bull. Amer. Meteorol. Soc.*, vol. 67, pp. 1150–1151, 1986.
[6] S. A. Changnon, "Midwestern cloud, sunshine and temperature trends since 1901: Possible evidence of jet contrail effects," *J. Appl. Meteorol.*, vol. 20, pp. 496–508, 1981.
[7] S. A. Changnon, R. G. Semonin, and W. M. Wendland, "Effect of contrail cirrus on surface weather conditions in the Midwest, Phase 1," Illinois Water Survey, Urbana, Final Rep. NSF, 1980, p. 141.
[8] J. Q. Degrand, A. M. Carleton, and P. J. Lamb, "A mid season climatology of jet condensation trails from high-resolution satellite data," Illinois Water Survey Rep., Urbana, 1991, pp. 25–30.
[9] A. G. Detwiler, "Comments on 'Jet contrails and cirrus clouds: A feasibility study employing high-resolution satellite imagery'," *Bull. Amer. Meteorol. Soc.*, vol. 67, pp. 1150–1151, 1986.
[10] A. G. Detwiler and R. Pratt, "Clear-air seeding: Opportunities and strategies," *J. Weath. Modif.*, vol. 16, pp. 46–60, 1984.
[11] R. O. Duda and P. E. Hart, "Use of the Hough transform to detect lines and curves in pictures," *Commun. ACM*, vol. 15, no. 1, pp. 11–15, 1972.
[12] M. Engelstad, S. K. Sengupta, T. Lee, and R. M. Welch, "Automated detection of jet contrails using the AVHRR split window," *Int. J. Remote Sensing*, vol. 13, no. 8, pp. 1391–1412, 1992.
[13] M. Ferland, "Les tainess of condensation," *Quebec Meteorol. Soc.*, vol. 14, pp. 695–718, 1975.
[14] R. C. Gonzalez and R. E. Woods, *Digital Image Processing.* New York: Addison-Wesley, 1992, p. 716.
[15] R. M. Haralick, "Ridges and valleys on digital images," *Comput. Vision, Graph., Image Processing*, vol. 22, pp. 28–38, 1983.
[16] P. V. C. Hough, "A method and means for recognizing complex patterns," U.S. Patent 3 069 654, 1962.
[17] J. C. Hurst, *The Image Processing Handbook*, 2nd ed. Greenwich, CT: CRC Press, 1995, p. 674.
[18] C. Johnson, J. Henshaw, and G. McInnes, "Impact of aircraft and surface emissions of nitrogen oxides on tropospheric ozone and global warming," *Nature*, vol. 355, pp. 69–71, 1992.
[19] J. H. Joseph, "Study of condensation trails observed from the ERTS-1 satellite imagery," *J. Geophys. Res.*, vol. 80, no. 3, pp. 366–372, 1975.
[20] J. H. Joseph, Z. Levin, Y. Mekler, G. Ohring, and J. Otterman, "Study of contrails observed from ERTS-1 satellite imagery," *J. Geophys. Res.*, vol. 80, no. 3, pp. 366–372, 1975.
[21] K. B. Kidwell, "NOAA polar orbiter data, user's guide," U.S. Dept. Commerce, NOAA NESDIS, Nat. Climate Data Center, Sat. Data Serv. Div., Washington, DC, p. 192, 1986.
[22] P. M. Kuhn, "Airborne observation of contrail effects on the thermal radiation budget," *J. Atmos. Sci.*, vol. 27, pp. 937–942, 1970.
[23] T. F. Lee, "Jet contrail identification using the AVHRR split window," *J. Appl. Meteorol.*, vol. 28, pp. 993–995, 1989.
[24] K. Lenggenhager, "Condensation trails from aircraft," *Zeitschrift fur Meteorologie*, Berlin, Germany, vol. 28, no. 6, pp. 368–373, 1978.
[25] M. Pitchford, J. G. Hudson, and J. G. Hallett, "Size and critical supersaturation for condensation of jet engine exhaust particles," *J. Geophys. Res.*, vol. 96, no. D11, vol. 20, pp. 787–20,793, 1991.
[26] W. K. Pratt, *Digital Image Processing.* New York: Wiley, p. 698.
[27] C. R. N. Rao, M. P. Weinreb, and J. Chen, "Recalibration of the Advanced Very High Resolution Radiometer for climate change research," *Adv. Space Res.*, vol. 14, pp. 117–120, 1994.
[28] R. S. Scorer, *Condensation Trails, Cloud Investigation by Satellite.* New York: Wiley, 1986.
[29] G. L. Stephens and P. J. Webster, "Clouds and climate: Sensitivity of simple systems." *J. Atmos. Sci.*, vol. 38, pp. 235–247, 1981.
[30] D. J. Travis, "Variations in contrail morphology and relationships to atmospheric conditions," *J. Weath. Mod.*, vol. 28, pp. 50–58, 1996.
[31] W. M. Wendland and R. G. Semonin, "Effect of contrail cirrus on surface weather conditions in the Midwest—Phase II," Illinois Water Survey, Champaign, Contract Rep. 298, 1982, p. 95.

John M. Weiss (M'89) received the B.A. degree in molecular biophysics and biochemistry from Yale University, New Haven, CT, in 1974, the Ph.D. degree in biochemistry from Vanderbilt University, Nashville, TN, in 1980, and the M.S. degree in computer science from Vanderbilt University in 1984.

He is with the Department of Mathematics and Computer Science, South Dakota School of Mines and Technology, Rapid City. He has published articles in many areas, including protein biochemistry, neuroanatomy, statistics and operations research, robotics, biomedical imaging, IFSAR-based photogrammetry, and satellite image processing. His current research interests focus on image processing, computer vision, and artificial intelligence.

Sundar A. Christopher received an engineering degree in Coimbatore, India, the M.S. degree in meteorology from the South Dakota School of Mines and Technology, Rapid City, and the Ph.D. degree in atmospheric sciences from Colorado State University, Fort Collins, in 1995.

He was with the Institute of Atmospheric Sciences, South Dakota School of Mines and Technology. He is now with the Department of Atmospheric Sciences, University of Alabama at Huntsville. His current research interests are satellite remote sensing of clouds, aerosols, jet contrails, biomass burning, and surface properties. He is a Member of the International SCaRaB scientific working group and a Science Advisor to the EOSDIS panel.

Ronald M. Welch received the B.S. and M.A. degrees in physics from California State University, Long Beach, and the Ph.D. degree in physics in 1971 and the Ph.D. degree in meteorology in 1976, both from the University of Utah, Salt Lake City.

He has been with the Department of Atmospheric Science, Colorado State University, Fort Collins, the Institute for Meteorology, Johannes Gutenberg University, Germany, Old Dominion University, Norfolk, VA, and the South Dakota School of Mines and Technology, Rapid City. Presently, he is Chair of Atmospheric Science at the Global Hydrology and Climate Center, University of Alabama at Huntsville. His research interests include global cloud and aerosol property retrievals, the earth radiative energy budget, 3-D cloud morphology analysis, and risk assessments of infectious disease spread due to short-term climate fluctuations.